THE JOURNAL OF PHYSICAL CHEMISTRY A

Subscriber access provided by University of East Anglia Library

A: Spectroscopy, Molecular Structure, and Quantum Chemistry

One- to Two-Exciton Transitions in Perylene Bisimide Dimer Revealed by Two-Dimensional Electronic Spectroscopy

Giovanni Bressan, Dale Green, Yohan Chan, Philip C. Bulman Page, Garth A. Jones, Stephen R. Meech, and Ismael A. Heisler

J. Phys. Chem. A, **Just Accepted Manuscript** • DOI: 10.1021/acs.jpca.8b11473 • Publication Date (Web): 05 Dec 2018

One- to Two-Exciton Transitions in Perylene Bisimide Dimer Revealed by Two-Dimensional Electronic Spectroscopy

Giovanni Bressan,[1] Dale Green[1], Yohan Chan,[1] Philip C. Bulman Page[1], Garth A. Jones[1], Stephen R. Meech[1] and Ismael A. Heisler[2,*]

[1]*School of Chemistry, Norwich Research Park, University of East Anglia, Norwich NR4 7TJ, United Kingdom*

[2]*Departamento de Física, Universidade Federal do Paraná, Caixa Postal 19044, 81531-990 Curitiba, Parana, Brazil*

*Corresponding author. Email: heisler@fisica.ufpr.br

Abstract

The excited state energy levels of molecular dimers and aggregates play a critical role in their photophysical behavior and an understanding of the photodynamics in such structures is critical when developing applications such as photovoltaics and optoelectronic devices. Here, exciton transitions in two different covalently bound PBI dimers are studied by two-dimensional electronic spectroscopy (2DES), a powerful spectroscopic method, providing the most complete picture of vibronic transitions in molecular systems. The data are accurately reproduced using the equation of motion-phase matching approach. The unambiguous presence of one-exciton to two-exciton transitions are captured in our results and described in terms of a molecular exciton energy level scheme based on the Kasha model. Furthermore, the results are supported by comparative measurements with the PBI monomer and another dimer in which the inter-chromophore distance is increased.

Introduction

Molecular structures based on the perylene bisimide (PBI) chromophore have been the object of extensive studies both from the perspective of fundamental photophysical properties, for instance, high emission yield[1,2], energy transfer[3,4,5], electron transfer[6,7] and singlet fission[8,9], as well as from the perspective of potential application in optoelectronic devices, such as optical sensors[10,11], solar light collectors[12,13] and optical power limiters[14]. Recently, properties of PBI aggregates have begun to be explored[15,16,17]. The aggregates may be prepared through chemical synthesis[18,19] or self-assembly[20,21] and exhibit interesting new photophysical properties, such as a red-shifted and spectrally narrowed main absorption peak as well as superradiance. To fully understand and explore the use of these newly synthesized supramolecular structures, it is necessary to determine the role and mechanism of electronic coupling and how it affects exciton dynamics. Such information is critical for the development of more efficient opto-electronic and photovoltaic devices.

The electronic structure of such covalently linked molecular dimers was first described[22] by Kasha more than fifty years ago. Electronic coupling between two (or more) chromophores creates Frenkel delocalized exciton states. Photophysically, this excitonic coupling translates into energy shifts of the absorption peaks and alterations of the radiative decay rate compared to uncoupled chromophores[23]. The sign of the spectral shift depends on the geometry. In H-dimers, the transition dipole moments are aligned “side-by-side”, producing a higher (lower) energy state related to the in- (out of-) phase coupling of the transition dipole moments. The radiative decay rate is enhanced (suppressed) for the higher (lower) energy states, leading to a spectral blue shift and suppressed emission. The opposite behavior is shown by so called J-aggregates: the in-phase condition, for the “head-to-tail” arrangement of the molecular transition dipole moments is lower in energy than the excited state of the uncoupled molecules, leading to a spectral red-shift and enhanced radiative decay rate of the lower energy state[24].

The coupling of chromophores to produce delocalized one-exciton states is necessarily accompanied by formation of two-exciton states, located at approximately twice the one-exciton energy. The one- to two-exciton excited state absorption (ESA) is blue-shifted compared to the one exciton transition due to the Pauli exclusion principle[25,26,27,28] , and this shift can be employed to determine the delocalization length of the excitons[26]. It is important to characterize the energetics and dynamics of two exciton states, because they can contribute to unwanted and detrimental exciton-exciton annihilation (EEA) processes in light-harvesting structures, materials and optoelectronic devices [29].

In this work we study the exciton structure of two covalently bound PBI dimers by two-dimensional electronic spectroscopy (2DES). 2DES provides a complete picture of vibronic[30,31] and inter-chromophore[32,33] coupling in molecular and biomolecular assemblies and it was previously employed to study excitonic states and relaxation dynamics in PBI heterodimers[34]. We demonstrate unambiguously the presence of a one to two-exciton state transition in the most strongly coupled dimer. The results are supported by comparative measurements with the PBI monomer and another dimer in which the inter-chromophore distance is increased and hence the electronic coupling is reduced. These data are then accurately reproduced by theoretical simulations of 2DES with purely electronic coupling. In this manner a detailed description of exciton delocalization in PBI aggregates emerges.

Experimental and Theoretical Methods

The 2D experimental setup has been described in detail before[35]. Briefly, the ultrafast pulses are generated in a commercial (TOPAS White - Light Conversion) noncollinear optical parametric amplifier (NOPA) pumped by a commercial amplifier (Spitfire Ace – Spectra Physics). The pulses are recompressed close to the Fourier transform limit at the sample position with a folded prism compressor, and characterized by transient grating frequency

resolved optical gating (TG-FROG) using a 1 mm cell with neat cyclohexane (typical TG-FROG pulsewidth 30 fs FWHM, FROG trace shown in the SI).

The 2D setup is designed in a fully noncollinear geometry, the four phase coherent beams are generated with a pair of beamsplitters and located at the corners of a 2.5 cm square. To acquire a 2D map the coherence time is scanned from – 150 fs to +150 fs in 4 fs steps. The data are phased according to the projection-slice theorem[36], which requires the acquisition of a transient absorption spectrum for each population time, this is done by blocking beams 1 and 3 and using the LO beam as probe.

The PBI monomer and dimer structures are shown in Figure 1a and SI (where the long – $C(C_9H_{19})_2$ aklylic chains, added at the imide positions to improve solubility and prevent aggregation, are shown) and were synthesised as reported previously[37,38,39].

The PBI monomer is modelled as a two level system with a ground, $|g\rangle$, and excited state, $|e\rangle$, separated by the transition frequency, $\tilde{\nu}_{eg}$, such that the Hamiltonian is defined by,

$$H_{\text{mon}} = |g\rangle\langle g| + hc\tilde{\nu}_{eg}\,|e\rangle\langle e| \tag{2}$$

and the dipole moment operator,

$$\hat{\mu}_{\text{mon}} = |\vec{\mu}|\left(|g\rangle\langle e| + |e\rangle\langle g|\right) \tag{3}$$

For the dimer systems, the monomers are considered point dipoles, $\vec{\mu}_{1/2}$, separated by the vector $\vec{R} = R\hat{R}$. Both dimers are *J*-aggregates, with collinear transition dipole moments which are also collinear with the displacement vector. The dipole coupling is given by the Förster equation,

$$J = \frac{\vec{\mu}_1 \cdot \vec{\mu}_2 - 3\left(\vec{\mu}_1 \cdot \hat{R}\right)\left(\vec{\mu}_2 \cdot \hat{R}\right)}{4\pi\varepsilon_r\varepsilon_0 R^3} \tag{4}$$

where ε_0 is the vacuum permittivity and ε_r is the relative permittivity of the solvent[40].

The diabatic dimer Hamiltonian is constructed as a composite Hilbert space, with the singly excited states, corresponding to an excitation on either monomer (1) or (2), coupled by *J*.

$$H_{\mathrm{dim}} = H_{\mathrm{mon}}^{(1)} \otimes I_{\mathrm{mon}}^{(2)} + I_{\mathrm{mon}}^{(1)} \otimes H_{\mathrm{mon}}^{(2)} + J\left(|e^{(1)}\rangle|g^{(2)}\rangle\langle g^{(1)}|\langle e^{(2)}| + |g^{(1)}\rangle|e^{(2)}\rangle\langle e^{(1)}|\langle g^{(2)}|\right) \tag{5}$$

Here I_{mon} is the identity operator over the monomer degrees of freedom[41].

The dimer Hamiltonian is then diagonalised via a unitary transformation into the adiabatic exciton basis. The diabatic dipole moment operator for the dimer system,

$$\hat{\mu}_{\mathrm{dim}} = \sqrt{\left|\vec{\mu}_1\right|^2 + \left|\vec{\mu}_2\right|^2}\left(\hat{\mu}_{\mathrm{mon}}^{(1)} \otimes I_{\mathrm{mon}}^{(2)} + I_{\mathrm{mon}}^{(1)} \otimes \hat{\mu}_{\mathrm{mon}}^{(2)}\right) \tag{6}$$

is also projected into the adiabatic exciton basis with the same unitary transformation.

Interaction with the solvent environment is defined using the hierarchical equations of motion (HEOM)[42,43]. Dephasing induced by fluctuations of the electronic transition frequencies is introduced by coupling the system to a bath of harmonic oscillators, described by the overdamped Drude spectral density,

$$J(\omega) = 2\eta\frac{\omega\gamma}{\omega^2 + \gamma^2} \tag{7}$$

Here γ defines the timescale of the fluctuations and η is the reorganisation energy of the bath.

The evolution of the system is defined in terms of an hierarchy of auxiliary density operators (ADO), $\rho_{\mathbf{j}}$, according to,

$$\dot{\rho}_{\mathbf{j}}(t) = -\left(\frac{i}{\hbar}H_S^{\times} + \sum_{k=0}^{M}\mathbf{j}_k\nu_k\right)\rho_{\mathbf{j}}(t) - i\sum_{k=0}^{M}B^{\times}\rho_{\mathbf{j}_k^+}(t) - i\sum_{k=0}^{M}\mathbf{j}_k\left(c_k B\rho_{\mathbf{j}_k^-}(t) - c_k^*\rho_{\mathbf{j}_k^-}(t)B\right) - \left(\frac{2\eta}{\hbar\beta\gamma} - \eta\cot\left(\frac{\hbar\beta\gamma}{2}\right) - \sum_{k=1}^{M}\frac{c_k}{\nu_k}\right)B^{\times}B^{\times}\rho_{\mathbf{j}}(t) \tag{8}$$

where $H_S^{\times}\rho = [H_S, \rho]$ denotes the commutator of the system Hamiltonian, $H_S = H_{\text{mon/dim}}$, and the density matrix, and the Matsubara frequencies, $\nu_k; k = 0,1,2,...,M$ and exponential prefactors, c_k, are,

$$\nu_0 = \gamma, \quad \nu_k = \frac{2\pi k}{\mathsf{h}\beta}, \quad c_0 = \eta\gamma\left(\cot\left(\frac{\mathsf{h}\beta\gamma}{2}\right) - i\right), \quad c_k = \frac{4\eta\gamma}{\mathsf{h}\beta}\left(\frac{\nu_k}{\nu_k^2 - \gamma^2}\right)$$

The system-bath coupling operators for pure dephasing are given by,

$$B_{\text{mon}} = |g\rangle\langle g| - |e\rangle\langle e| \tag{9}$$

$$B_{\text{dim}} = |g\rangle\langle g| - |e'\rangle\langle e'| - |e''\rangle\langle e''| - 3|f\rangle\langle f| \tag{10}$$

The ADOs account for non-Markovian memory effects within the evolution, related to the amount of static disorder and inhomogeneous broadening. They are distinguished by the $(M+1)$-dimensional vectors $\mathbf{j} = (j_{10}, \ldots, j_k, \ldots, j_M)$ and $\mathbf{j}^{\pm} = (j_{10}, \ldots, j_k \pm 1, \ldots, j_M)$, which contain elements for each Matsubara frequency. The coefficients of these elements, j_k, define the depth of the hierarchy, where the ADO with all coefficients equal to zero is equivalent to the true reduced density matrix.

The hierarchy is terminated by selection of an appropriate convergence parameter, Γ, such that the number of Matsubara frequencies is selected according to,

$$\frac{2(M+1)\pi}{\mathsf{h}\beta} > \Gamma \tag{11}$$

and the number of ADOs is determined by,

$$\sum_{k=0}^{M} \mathbf{j}_k \nu_k > \Gamma \tag{12}$$

Here we set $\Gamma = 10\gamma$, assuming any faster fluctuations evolve within the Markovian limit. The fourth order Runge-Kutta numerical integration method is used to solve eq. 7, with a step size of 0.05 fs.

The 2D-ES spectra are calculated using the equation of motion-phase matching approach (EOM-PMA)[44,45]. The third order polarization in the rephasing, $\mathbf{k}_s = -\mathbf{k}_1 + \mathbf{k}_2 + \mathbf{k}_3$, or non-rephasing, $\mathbf{k}_s = \mathbf{k}_1 - \mathbf{k}_2 + \mathbf{k}_3$, direction is calculated by,

$$P^{(3)}_{\mathbf{k}_s}(\tau, T, t) = e^{i\mathbf{k}_s \mathbf{r}} \mathbf{Tr}[\hat{\mu}(\rho_1(t) - \rho_2(t) - \rho_3(t) + \rho_4(t) - \rho_5(t) + \rho_6(t) + \rho_7(t))] + c.c. \quad (13)$$

where $\rho_i(t); i = 1, 2, \ldots, 7$ are additional non-Hermitian auxiliary density operators, evolved using eq. 7, for which the system Hamiltonian has been extended to include one of seven arrangements of time-dependent terms,

$$H_1 = H_S - V_1(t) - V_2^{\dagger}(t) - V_3^{\dagger}(t) \quad (14)$$

$$H_2 = H_S - V_1(t) - V_2^{\dagger}(t) \quad (15)$$

$$H_3 = H_S - V_1(t) - V_3^{\dagger}(t) \quad (16)$$

$$H_4 = H_S - V_1(t) \quad (17)$$

$$H_5 = H_S - V_2^{\dagger}(t) - V_3^{\dagger}(t) \quad (18)$$

$$H_6 = H_S - V_2^{\dagger}(t) \quad (19)$$

$$H_7 = H_S - V_3^{\dagger}(t) \quad (20)$$

These time-dependent Hamiltonians incorporate the interaction with the three electric fields through the operators $V_m(t)$: $m = 1, 2, 3$,

$$V_m(t) = \left(\hat{\mu}\chi_m E_m(t - \tau_m)\exp(-i\omega_m t)\right) \quad (21)$$

where $\omega_m = 2\pi\nu_m$ has the associated wavevector, $\mathbf{k}_m$, χ_m is the electric field strength and the field envelope, $E(t-\tau_m)$ centred at τ_m, is assumed to be Gaussian.

Each EOM-PMA auxiliary describes a number of Liouville pathways, such that their combination in eq. 12 isolates the pathways in the phase matched direction. Further details can be found in the SI of reference[43].

The rephasing, S_R, and non-rephasing, S_{NR}, 2D spectra are then produced as the double Fourier transform of the third order polarization[46],

$$S_R(\omega_\tau, T, \omega_t) = \int_0^\infty dt \int_0^\infty d\tau \exp[-i\omega_\tau \tau] \exp[+i\omega_t t] i P_R^{(3)}(\tau, T, t) \tag{22}$$

$$S_{NR}(\omega_\tau, T, \omega_t) = \int_0^\infty dt \int_0^\infty d\tau \exp[+i\omega_\tau \tau] \exp[+i\omega_t t] i P_{NR}^{(3)}(\tau, T, t) \tag{23}$$

and summed to give the absorptive spectrum,

$$S_A = \mathbf{Re}\left(S_R + S_{NR}\right) \tag{24}$$

All *ab initio* calculations were performed with Gaussian09.[47] Molecules M, D0 and D1 were optimized with the B3LYP functional and the 6-31G* basis set. All structures were shown to be genuine minima, via a harmonic vibrational analysis (all real frequencies). Relevant vibrational modes are presented in the SI.

Results and Discussion

The molecular structures of the PBI molecules studied are presented in Figure 1a, where the monomer M (top), dimers D0 (center) and D1 (bottom) are shown (aliphatic side chains required for solubility in the actual molecules studied are omitted for clarity – see supplementary information, SI). In the D0 dimer, in which the center to center distance *R* is 12.7 Å[19], the PBI units are connected by an N-N bond at the imide position, forcing the two PBI to lie on two perpendicular planes. For the D1 dimer, the PBI units are linked at the imide

N position through a *p*-phenylene spacer. As a result the center to center distance *R* is increased to 17 Å[19] and the molecule can explore a wider distribution of conformations.

The visible absorption data for the three PBI structures in toluene are shown in Figure 1b. The spectrum of M exhibits a characteristic vibronic progression built on the $S_0 \rightarrow S_1$ (527 nm) transition. A detailed analysis was performed by Clark et al[48], where they showed that the vibronic progression comprises normal vibrational modes $\nu_{12} = 231 cm^{-1}$ (in-plane ν_{C-C}), $\nu_{30} = 550 cm^{-1}$ (in-plane δ_{C-C-C}), $\nu_{77} = 1308 cm^{-1}$ (in-plane ν_{C-C}, δ_{C-H}) and $\nu_{100} = 1660 cm^{-1}$ (in-plane ν_{C-C}), plus combination bands.

The spectrum of the dimer D0 shows significant new features. First, its $S_0 \rightarrow S_1$ transition is red-shifted by 9 nm to 536 nm compared to M. Second, the amplitude ratio between the pure $S_0 \rightarrow S_1$ electronic transition ($I_{0,0}$) and its first vibronic peak ($I_{0,1}$)i. e., $I_{0,0}/ I_{0,1}$, is enhanced compared to M. The D1 dimer spectrum has an $S_0 \rightarrow S_1$ electronic transition at approximately the same wavelength as M (527 nm) and has a similar profile, but it is broadened towards shorter wavelengths.

Figure 2a presents the experimental absorptive 2DES spectra at T = 0.1 ps for M (left), D0 (middle) and D1 (right), while the corresponding simulated absorptive 2DES spectra are shown in Figure 2b. In the 2DES spectra, the positive signals (red colours) correspond to the ground state bleaching (GSB) and/or stimulated emission (SE), whereas the negative (blue colours) correspond to excited state absorption (ESA).

For M (Figure 2a, left), the 2DES spectrum shows no negative contribution, i.e., there is no evidence of ESA. The signal can be described as having GSB/SE contributions exclusively in the studied spectral region accessible by the laser spectrum. The elongation towards small $\tilde{\nu}_3$ values coincides with the position of the fluorescence spectrum (see SI) so is assigned to a SE contribution. There is a small elongation of the 2DES spectra along the diagonal, indicating

that a degree of inhomogeneous broadening is present. The spectral reshaping that occurs within the first 10 ps (shown by the sequence of 2DES spectra reported for each molecule in the SI) is assigned to spectral diffusion. Furthermore, within the first few picoseconds it is possible to observe the Stokes shift evolving, a signature of vibrational cooling processes taking place in the electronic excited state potential energy surface, whose detailed characterization is beyond the scope of this work.

The dimer D0 (Figure 2a, center), apart from being down-shifted in energy, shows a striking new feature given by an ESA off-diagonal peak (centered at $\tilde{\nu}_1 = 18612\ \mathrm{cm}^{-1}, \tilde{\nu}_3 = 19202\ \mathrm{cm}^{-1}$), which is absent in M. In contrast, the dimer D1 (Figure 2a, right) has a 2DES spectrum more closely resembling that of M, i.e., showing only GSB/SE contributions and with its main electronic transition at approximately the same wavelength as M ($\tilde{\nu}_1 = 19875\ \mathrm{cm}^{-1}, \tilde{\nu}_3 = 19875\mathrm{cm}^{-1}$), but broadened, as already noted in the linear absorption spectra.

The photophysical behavior for this series of molecules can be rationalized and understood in terms of the proposed energy level scheme shown in Figure 3a, which is based on the Kasha exciton model. In the dimer, the two monomers are arranged in a "head-to-tail" fashion and, therefore, the coupling mechanism is given by a *J*-coupling scheme. A new fully allowed transition (solid arrow in Figure 3a) to the bottom exciton state (e') occurs in the dimer whereas a forbidden transition (dashed arrow in Figure 3a) to the upper exciton state (e") is suppressed and cannot contribute to the linear and nonlinear absorption spectra. This low energy transition accounts for the red-shift observed in the linear absorption of D0. For D1, the center-to-center distance between the monomer units is larger than for D0, making the excitonic coupling much weaker in this dimer, as reflected in the absence of red-shifting in the linear absorption.

The proposed energy level scheme also explains the prominent new ESA contribution seen in the 2DES spectra for D0. Once a population, $|e'\rangle\langle e'|$, is created in the lower exciton (e') state

via the first two field-matter interactions, a third laser pulse can excite the transition to the higher energy two-exciton state (f), which gives rise to the ESA (negative signal), observed exclusively in the D0 dimer 2D spectrum. The Feynman diagrams accounting for the three field-matter interactions which generate this signal in the predicted positions of the 2DES spectra are shown in the SI[49].

The excitonic coupling strength, *J*, in D0, can be determined by the spectral separation between the positive GSB transition (g→ e') and the negative ESA transition (e'→f) observed in the 2DES spectra. Figure 3b shows a vertical cut for a fixed excitation frequency (at $\tilde{\nu}_1 = 18682$ cm^{-1}) applied to the absorptive 2D map of D0 in toluene (shown in Figure 2b). This frequency was specifically chosen because it corresponds to maxima of absorption for a specific excitation frequency, marked with squares in Figure 2a. Thus the contrast between the amplitude of the positive and negative peaks is maximized. However it is important to point out that the value for the excitonic coupling strength is not dependent on choosing one specific frequency, although the error in its evaluation is minimized by determining the frequency difference of the absorption maxima as done here.

The dashed lines in Figure 3b show the maxima of the positive and the negative peaks and the spectral separation is given by 520 cm^{-1}, which corresponds to 2*J*. Therefore, the interaction energy is given by $J = 260$ cm^{-1} that is in reasonable agreement with the spectral shift observed in the linear absorption spectrum (Figure 1b, $\Delta\tilde{\nu} =$ 300 cm^{-1}) and reported in literature[19].

As already noted, the prominent ESA band observed in the 2DES spectra of D0 is absent in the 2DES spectra of D1 and M (Figure 2a, right and left). As this spectral feature was assigned to one to two-exciton state transitions in D0, this implies excitonic coupling is weaker or absent in D1. This is expected as the distance between the PBI monomers increases by more than 30% compared to D0. The interaction energy, assuming a Förster-type coupling scheme, scales with

the inverse of distance to the third power, $J \alpha R^{-3}$. Therefore the interaction energy for D1, J_{D1}, should be about 0.4 that of D0, i. e., $J_{D1} = 0.4\ J_{D0}$. This would translate into about $J_{D1} = 100$ cm^{-1}. This is in good agreement with the calculated spectrum for D1, where the weaker coupling results in a much smaller down-shift (108.4 cm^{-1}, see below) with the bulk of the ESA peak being obscured by the GSB/SE peak.

For the calculated spectra (Figure 2b), M was defined with $\nu_{eg} = 18939$ cm^{-1} and $|\vec{\mu}| = 11.218$ Debye, such that for D0 with $R = 1.27$ nm, $J = -260.0$ cm^{-1} and for D1 with $R = 1.7$ nm, $J = -108.4$ cm^{-1}, where $\varepsilon_r = 2.38$ for toluene[50]. All simulations were completed at 298 K, with $\eta = 20$ cm^{-1} and $\gamma = 75$ cm^{-1}. The laser spectra were centred at $\nu_m = c\nu_{eg}$ for the monomer and $\nu_m = c\nu_{e'g}$ for the dimers, with FWHM of 5 fs and $\chi_m = 1 \times 10^7$ Vm^{-1}.

The calculated spectra reproduce the positive GSB/SE features and the inhomogeneous broadening of M (Figure 2b, left). The elongation about $\tilde{\nu}_3$ observed in the experimental spectrum is due to vibrational modes not included in the theoretical model, hence is absent from the calculated spectrum. The red-shift of the g $\rightarrow$ e' transition and emergence of the one to two-exciton ESA due to coupling, both in D0 and D1 (Figure 2b, center and right), is also reproduced. However, due to a higher degree of flexibility, D1 is more disordered than D0, as seen in the linear absorption spectrum. Hence the ESA in the experimental 2DES spectrum for D1 (Figure 2a, right) is obscured. Such disorder tends to disrupt coherent excitonic coupling. The amount of static disorder was kept fixed across the M, D0, and D1 series to demonstrate the weakening of the dipole-dipole coupling due to increased separation distance, as predicted in the Kasha model.

The dynamics of the ESA cross peak in D0 mirrors that of the GSB. This can be seen in Figure 4a, where the temporal evolution of the GSB+SE (blue circles) and ESA (green triangles)

integrated signals are shown. These plots were obtained integrating a square sized 150 x 150 $(cm^{-1})^2$ of the D0 2D spectrum around the positive (blue square) and negative (green square) maxima, as shown in Figure 2a. These curves can be fit with a sum of two exponential functions and the recovered time constants are very similar. The shortest decay time is around a picosecond and can be assigned to vibrational cooling, whereas the long decay constant around 600 ps can be assigned to population relaxation. Similar vibrational cooling dynamics are occurring on a sub-ps scale in M and D1 as well, those are revealed by the spectral reshaping occurring within this time window (see the top row of spectral progressions from 0.1 ps to 300 ps in the Supplementary Information).

In D0, there is no indication of energy transfer (even at early times) from the upper (e") to the lower (e') exciton states, confirming the fact that the upper state is connected to the ground state by a completely dipole forbidden transition. Further confirmation is given by the absence of any coherent oscillating signal between the upper (e") and lower (e') exciton states. Such a coherence would show as an oscillation with a sub-100 fs dephasing time during T and as a broad signal centered around 520 cm^{-1} in the frequency domain. Figure 4b shows the power spectrum amplitude for the rephasing 2DES signal obtained by integrating the 2DES spectra over $\tilde{\nu}_1$ and $\tilde{\nu}_3$ to generate a single curve as a function of population time, over which a FFT is taken. For M, (Figure 4b, red line) the main contributing frequencies are a broad band at frequencies below 250 cm^{-1} and a narrow band at 532 cm^{-1}(C-C-C in plane bending of the PBI core).

The power spectrum of D0 (Figure 4b, blue line) can be fully explained in terms of multiple vibronic oscillations occurring during T. For this dimer a new low frequency mode (~100 cm^{-1}) N-N stretching (not present either in M or D1) is predicted from DFT calculations (see SI for full details). A narrowband medium intensity signal is indeed present at this frequency in the experimental FT spectrum of D0. Again, the strongest signal is the C-C-C in-plane bending

observed in M, slightly blue-shifted in D0 ($\Delta v = 18$ cm^{-1}) (FT amplitude maps of the 550, 532 and 100 cm^{-1} modes in the Rephasing spectra of M and D0 are shown in the SI). The quasi-resonance between vibronic and excitonic splittings might be expected to result in coherence transfer between the two superpositions. However, the picosecond coherence lifetime and the narrow bandwidth of the peak at 550 cm^{-1} confirm that the nature of this oscillation is completely vibronic.

Conclusions

In summary, exciton transitions in two covalently bound PBI dimers were studied with 2DES. The unambiguous presence of one-exciton to two-exciton state transitions are captured in the dimer with the shortest distance between the monomer units D0 (strongest coupling). This dimer shows an energy down-shifted transition (compared to M), and the one to two-exciton state transition appears as an ESA off-diagonal peak (centred at $\tilde{\nu}_1 = 18612$ cm^{-1}, $\tilde{\nu}_3 = 19202$ cm^{-1}), which is absent in M and D1. This new spectral feature can be explained in terms of a molecular exciton energy level scheme based on the Kasha model and is theoretically corroborated with the equation of motion-phase matching approach.

Supporting Information

Molecular structures, steady-state fluorescence and 2DES spectral progressions for M, D0 and D1 in Toluene; Double-sided Feynman diagrams; DFT calculations for M, D0 and D1, Rephasing FT amplitude maps for M , D0 and D1 and TG-FROG trace.

Acknowledgments

This work was supported by EPSRC grants EP/P01111X/1, EP/J009148/1 and J021431/1. The theoretical calculations were carried out on the High Performance Computing Cluster supported by the Research and Specialist Computing Support service at the University of East Anglia.

Figure Captions

Fig. 1 (a) Molecular structures of the PBI molecules studied. Monomer M and dimers D0 and D1; alkyl chains are added to improve solubility (See SI). (b) Normalized steady-state absorption (solid lines) spectra of M, D) and D1 in toluene.

Fig. 2 Measured (a) and calculated (b) 2D-ES absorptive spectra for M (left), D0 (center) and D1 (right) samples in toluene at population time T = 0.1 ps (for later times see SI). Each 2D spectrum is normalised to its maximum and the amplitude has 21 evenly spaced contour lines. A blue and a green square highlight the area which was integrated in order to obtain the time traces shown in Figure 4 (b). In 2a (experimental data) the top panels are showing the steady-state absorption (red line) and the NOPA spectrum (blue line). In 2b the calculated spectra are normalized to their maxima and the amplitude has 21 evenly spaced contour lines. The top panels are showing the steady-state absorption data (red line).

Fig. 3 (a) Jablonski diagram showing energy levels and transitions for a PBI monomer (left) and excitonically coupled J-type dimer (right). Solid arrows represent allowed transitions and dashed arrows represent forbidden transitions. The energy difference between the bottom e' (allowed) and the top e" (forbidden) exciton states corresponds to 2J. (b) Vertical cut for a fixed excitation frequency (at $\tilde{\nu}_1 = 18682$ cm^{-1}) applied to the absorptive 2D map of D0 in toluene shown in Figure 2b. Therefore the frequency axis of this Figure corresponds the $\tilde{\nu}_3$ axis of Figure 2b. The dashed lines are highlighting the energy difference between the maximum of the positive (GSB + SE region) and the minimum of the negative (ESA region) signals, which is proportional to the excitonic splitting.

Fig. 4 (a) Temporal evolutions of the integrated amplitude on a 150 cm^{-1} side square centered at the GSB + SE positive maximum (blue circles) and ESA negative minimum (green triangles). Red and orange solid lines are the multi (2) exponential fits of the integrated amplitudes vs T

(ps). The recovered time constants are similar and they do suggest that the two transitions share a common state (e').

(b) Power spectrum of the residuals of the 2D global fit of rephasing signals of M (red) and D0 (blue), after integration over the excitation and detection axes. M shows one main contribution at 532 cm^{-1}, assigned to a C-C-C in plane bending mode. The same mode, blue-shifted of 20 cm^{-1}, contributes to the power spectrum of D0, and for this molecule a new low frequency vibrational mode is assigned to the imide N-N stretching at 100 cm^{-1}.

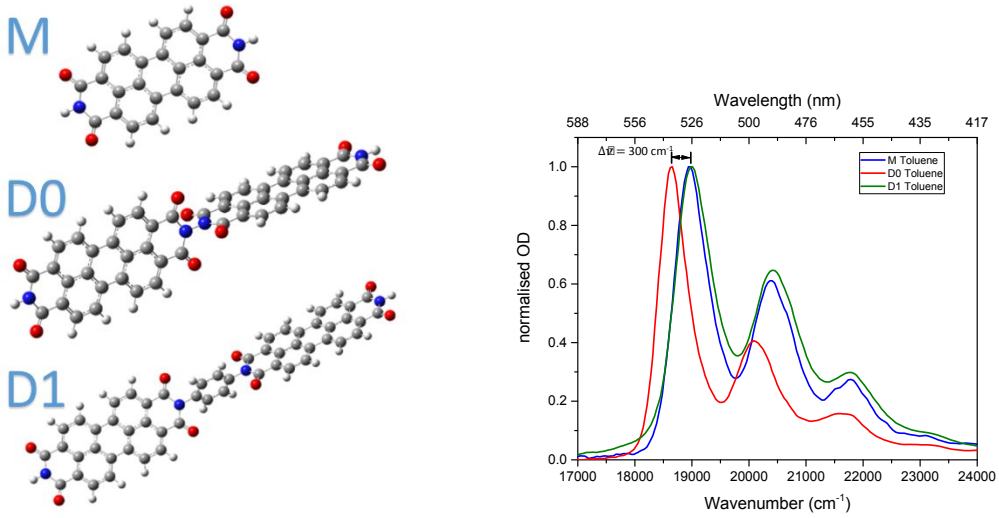
M
D0
D1
Wavelength (nm)
588 556 526 500 476 455 435 417
Δν̄ = 300 cm⁻¹
M Toluene
D0 Toluene
D1 Toluene
normalised OD
1.0 0.8 0.6 0.4 0.2 0.0
17000 18000 19000 20000 21000 22000 23000 24000
Wavenumber (cm⁻¹)

(a) (b)

Figure 1

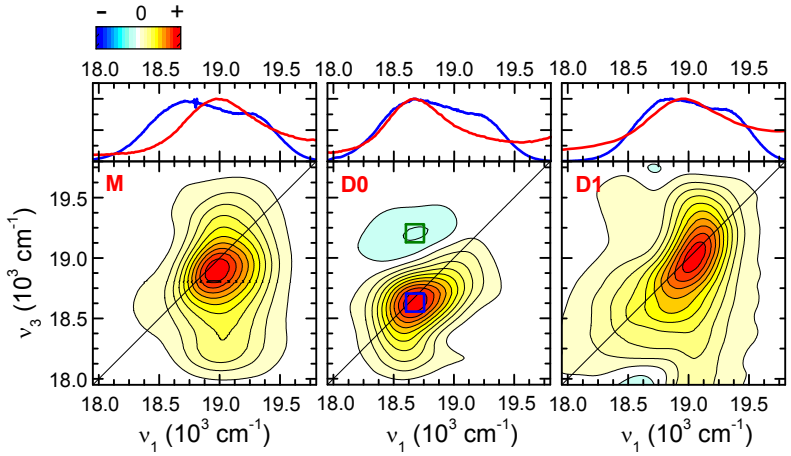

(a)

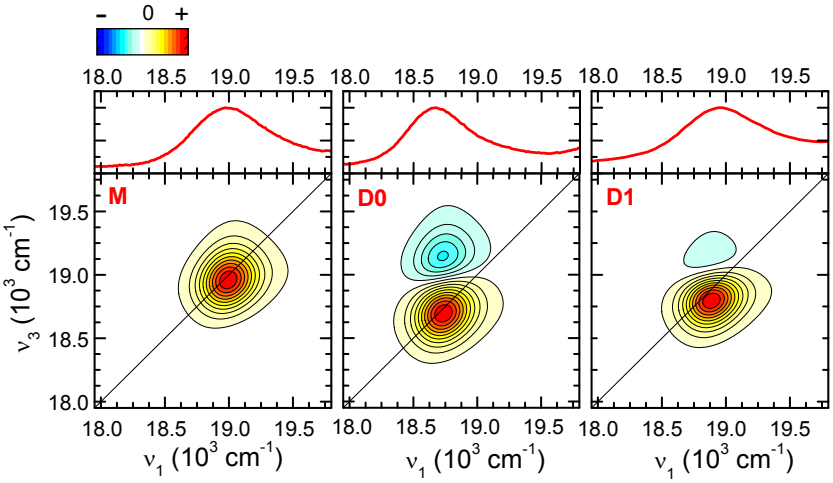

(b)

Figure 2

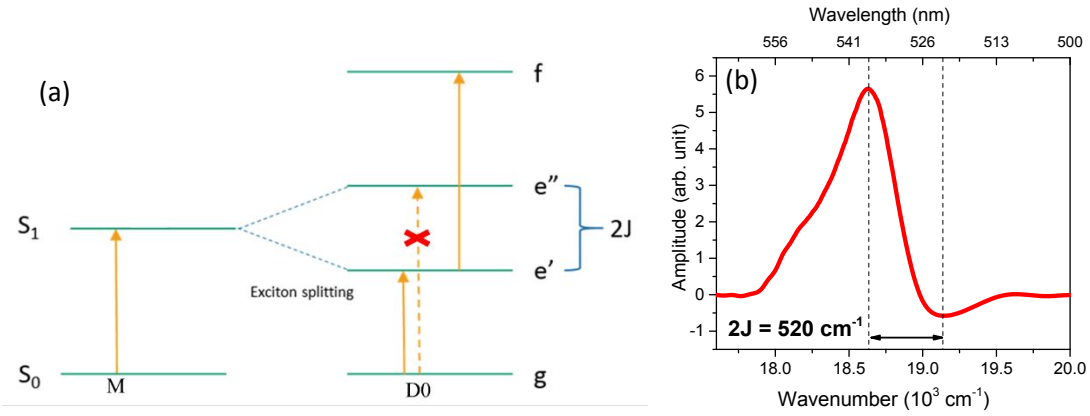
(a)
f
e″
e′
2J
S1
S0
M
D0
g
Exciton splitting
(b)
Wavelength (nm)
556
541
526
513
500
Amplitude (arb. unit)
2J = 520 cm-1
Wavenumber (10^3 cm^-1)

Figure 3

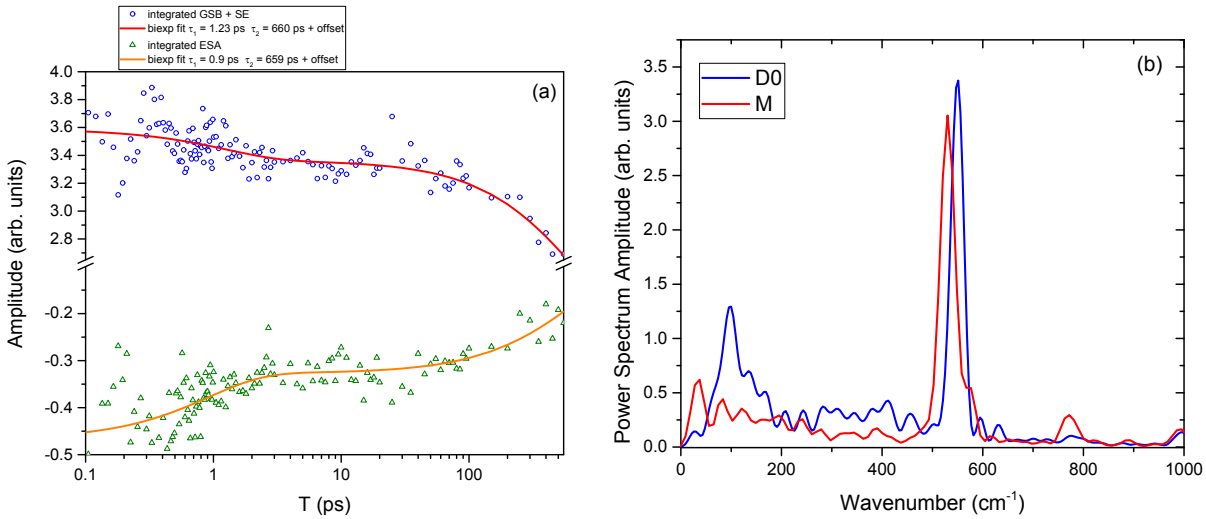
integrated GSB + SE
biexp fit τ1 = 1.23 ps τ2 = 660 ps + offset
integrated ESA
biexp fit τ1 = 0.9 ps τ2 = 659 ps + offset
(a)
Amplitude (arb. units)
T (ps)
(b)
D0
M
Power Spectrum Amplitude (arb. units)
Wavenumber (cm-1)

Figure 4

References

(1) Zhao, Q.; Zhang, S.; Liu, Y.; Mei, J.; Chen, S.; Lu, P.; Qin, A.; Ma, Y.; Sun, J. Z.; Tang, B. Z. Tetraphenylethenyl-Modified Perylene Bisimide: Aggregation-Induced Red Emission, Electrochemical Properties and Ordered Microstructures. *J. Mater. Chem.* **2012**, *22*, 7387–7394.

(2) Würthner, F. Bay-Substituted Perylene Bisimides: Twisted Fluorophores for Supramolecular Chemistry. *Pure Appl. Chem.* **2006**, *78*, 2341–2349.

(3) Wasielewski, M. R. Self-Assembly Strategies for Integrating Light Harvesting and Charge Separation in Artifical Photosynthetic Systems. *Acc. Chem. Res.* **2009**, *42*, 1910–1921.

(4) Hippius, C.; Schlosser, F.; Vysotsky, M. O.; Bhmer, V.; Wrthner, F.; Bo, V.; Wu, F. Energy Transfer in Calixarene-Based Cofacial-Positioned Perylene Bisimide Arrays Energy Transfer in Calixarene-Based Cofacial-Positioned Perylene Bisimide Arrays. *J. Am.Chem. Soc.* **2006**, *128*, 3870–3871.

(5) Pandya, R.; MacQueen, R. W.; Rao, A.; Davis, N. J. L. K. Simple and Robust Panchromatic Light Harvesting Antenna Composites via FRET Engineering in Solid State Host Matrices. *J. Phys. Chem. C* **2018**, *122*, 22330-22338..

(6) Zang, L.; Liu, R.; Holman, M. W.; Nguyen, K. T.; Adams, D. M. A Single-Molecule Probe Based on Intramolecular Electron Transfer. *J. Am. Chem. Soc.* **2002**, *124*, 10640–10641.

(7) Takada, T.; Ishino, S.; Takata, A.; Nakamura, M.; Fujitsuka, M.; Majima, T.; Yamana, K. Rapid Electron Transfer of Stacked Heterodimers of Perylene Diimide Derivatives in a DNA Duplex. *Chem. - A Eur. J.* **2018**, *24*, 8228–8232.

(8) Eaton, S. W.; Shoer, L. E.; Karlen, S. D.; Dyar, S. M.; Margulies, E. A.; Veldkamp, B. S.; Ramanan, C.; Hartzler, D. A.; Savikhin, S.; Marks, T. J.; et al. Singlet Exciton Fission in Polycrystalline Thin Films of a Slip-Stacked Perylenediimide. *J. Am. Chem. Soc.* **2013**, *135*, 14701–14712.

(9) Ramanan, C.; Smeigh, A. L.; Anthony, J. E.; Marks, T. J.; Wasielewski, M. R. Competition between Singlet Fission and Charge Separation in Solution-Processed Blend Films of 6,13-Bis(Triisopropylsilylethynyl)Pentacene with Sterically-Encumbered Perylene-3,4:9,10-Bis(Dicarboximide)S. *J. Am. Chem. Soc.* **2012**, *134*, 386–397.

(10) Feng, X.; An, Y.; Yao, Z.; Li, C.; Shi, G. A Turn-on Fluorescent Sensor for Pyrophosphate Based on the Disassembly of Cu2+-Mediated Perylene Diimide Aggregates. *ACS Appl. Mater. Interfaces* **2012**, *4*, 614–618.

(11) Wang, B.; Yu, C. Fluorescence Turn-on Detection of a Protein through the Reduced Aggregation of a Perylene Probe. *Angew. Chemie - Int. Ed.* **2010**, *49*, 1485–1488.

(12) Sugiyasu, K.; Fujita, N.; Shinkai, S. Visible-Light-Harvesting Organogel Composed of Cholesterol-Based Perylene Derivatives. *Angew. Chemie - Int. Ed.* **2004**, *43*, 1229–1233.

(13) Kirmaier, C.; Bocian, D. F.; Holten, D.; Lindsey, J. S.; Roy, A. Synthesis of Arrays Containing Porphyrin, Chlorin, and Perylene-Imide Constituents for Panchromatic Light-Harvesting and Charge Separation. *RSC Adv.* **2018**, *8*, 23854–23874.

(14) Kufazvinei, C.; Ruether, M.; Wang, J.; Blau, W. A Blue Light Emitting Perylene Derivative with Improved Solubility and Aggregation Control: Synthesis, Characterisation and Optical Limiting Properties. *Org. Electron. physics, Mater. Appl.* **2009**, *10*, 674–680.

(15) Potma, E. O.; Wiersma, D. a. Exciton Superradiance in Aggregates: The Effect of Disorder,

Higher Order Exciton-Phonon Coupling and Dimensionality. *J. Chem. Phys.* **1998**, *108*, 4894-4903.

(16) Würthner, F.; Saha-Möller, C. R.; Fimmel, B.; Ogi, S.; Leowanawat, P.; Schmidt, D. Perylene Bisimide Dye Assemblies as Archetype Functional Supramolecular Materials. *Chem. Rev.* **2016**, *116*, 962–1052.

(17) Brixner, T.; Hildner, R.; Köhler, J.; Lambert, C.; Würthner, F. Exciton Transport in Molecular Aggregates - From Natural Antennas to Synthetic Chromophore Systems. *Adv. Energy Mater.* **2017**, *7*, 1700236.

(18) Brown, K. E.; Salamant, W. A.; Shoer, L. E.; Young, R. M.; Wasielewski, M. R. Direct Observation of Ultrafast Excimer Formation in Covalent Perylenediimide Dimers Using Near-Infrared Transient Absorption Spectroscopy. *J. Phys. Chem. Lett.* **2014**, *5*, 2588–2593.

(19) Diehl, F. P.; Roos, C.; Duymaz, A.; Lunkenheimer, B.; Köhn, A.; Basché, T. Emergence of Coherence through Variation of Intermolecular Distances in a Series of Molecular Dimers. *J. Phys. Chem. Lett.* **2014**, *5*, 262–269.

(20) Balakrishnan, K.; Datar, A.; Naddo, T.; Huang, J.; Oitker, R.; Yen, M.; Zhao, J.; Zang, L. Effect of Side-Chain Substituents on Self-Assembly of Perylene Diimide Molecules: Morphology Control. *J. Am. Chem. Soc.* **2006**, *128*, 7390–7398.

(21) Sung, J.; Kim, P.; Fimmel, B.; Würthner, F.; Kim, D. Direct Observation of Ultrafast Coherent Exciton Dynamics in Helical π-Stacks of Self-Assembled Perylene Bisimides. *Nat. Commun.* **2015**, *6*, 8646.

(22) Kasha, M. Energy Transfer Mechanisms and the Molecular Exciton Model for Molecular Aggregates. *Radiat. Res.* **1963**, *20*, 55–70.

(23) Hestand, N. J.; Spano, F. C. Expanded Theory of H- and J-Molecular Aggregates: The Effects of Vibronic Coupling and Intermolecular Charge Transfer. *Chem. Rev.* **2018**, *118*, 7069-7163.

(24) Fidder, H.; Knoester, J.; Wiersma, D. A. Superradiant Emission and Optical Dephasing in J-Aggregates. *Chem. Phys. Lett.* **1990**, *171*, 529–536.

(25) Durrant, J. R.; Knoester, J.; Wiersma, D. A. Local Energetic Disorder in Molecular Aggregates Probed by the One-Exciton to Two-Exciton Transition. *Chem. Phys. Lett.* **1994**, *222*, 450–456.

(26) Johnson, A. E.; Kumazaki, S.; Yoshihara, K. Pump-Probe Spectroscopy and Exciton Dynamics of J Aggregates at High Pump Intensities. *Chem. Phys. Lett.* **1993**, *211*, 511–515.

(27) Fidder, H.; Knoester, J.; Wiersma, D. a. Observation of the One-Exciton to Two-Exciton Transition in a J Aggregate. *J. Chem. Phys.* **1993**, *98*, 6564-6566.

(28) Chen, X.; Kobayashi, T. The Effect of Two-Exciton States on the Linear Absorption of the Third Molecular Level in Linear Molecular Aggregates. *J. Chem. Phys.* **2002**, *117*, 11347–11351.

(29) Fidder, H.; Wiersma D. A.; Resonance-Light-Scattering Study and Line Shape Simulation of The *J* Band.*Phys. Rev. Lett.* **1991**, *66*, 1501–1504.

(30) Milota, F.; Prokhorenko, V. I.; Mancal, T.; Von Berlepsch, H.; Bixner, O.; Kauffmann, H. F.; Hauer, J. Vibronic and Vibrational Coherences in Two-Dimensional Electronic Spectra of Supramolecular J-Aggregates. *J. Phys. Chem. A* **2013**, *117*, 6007–6014.

(31) Anda, A.; Abramavičius, D.; Hansen, T. Two-Dimensional Electronic Spectroscopy of Anharmonic Molecular Potentials. *Phys. Chem. Chem. Phys.* **2018**, *20*, 1642–1652.

(32) Fassioli, F.; Dinshaw, R.; Arpin, P. C.; Scholes, G. D. Photosynthetic Light Harvesting : Excitons and Coherence Photosynthetic Light Harvesting : Excitons and Coherence. *J. R. Soc. Interface* **2014**, *11*, 20130901.

(33) Fuller, F. D.; Ogilvie, J. P. Experimental Implementations of Two-Dimensional Fourier Transform Electronic Spectroscopy. *Annu. Rev. Phys. Chem.* **2015**, *66*, 667–690.

(34) Selig, U.; Nuernberger, P.; Dehm, V.; Settels, V.; Gsänger, M.; Engels, B.; Würthner, F.; Brixner, T. Similarities and Differences in the Optical Response of Perylene-Based Hetero-Bichromophores and Their Monomeric Units. *ChemPhysChem* **2013**, *14*, 1413–1422.

(35) Heisler, I. A.; Moca, R.; Camargo, F. V. A.; Meech, S. R. Two-Dimensional Electronic Spectroscopy Based on Conventional Optics and Fast Dual Chopper Data Acquisition. *Rev. Sci. Instrum.* **2014**, *85*, 063103.

(36) Brixner, T.; Mančal, T.; Stiopkin, I. V.; Fleming, G. R. Phase-Stabilized Two-Dimensional Electronic Spectroscopy. *J. Chem. Phys.* **2004**, *121*, 4221–4236.

(37) Langhals, H.; Jona, W. Intense Dyes through Chromophore-Chromophore Interactions: Bi- and Trichromophoric Perylene-3,4:9,10-Bis(Dicarboximide)S. *Angew. Chemie - Int. Ed.* **1998**, *37*, 952–955.

(38) Wicklein, A.; Lang, A.; Muth, M.; Thelakkat, M. Swallow-Tail Substituted Liquid Crystalline Perylene Bisimides: Synthesis and Thermotropic Properties. *J. Am. Chem. Soc.* **2009**, *131*, 14442–14453.

(39) Wescott, L. D.; Mattern, D. L. Donor-σ-Acceptor Molecules Incorporating a Nonadecyl-Swallowtailed Perylenediimide Acceptor. *J. Org. Chem.* **2003**, *68*, 10058–10066.

(40) Hestand, N. J.; Spano, F. C. Expanded Theory of H- and J-Molecular Aggregates: The Effects of Vibronic Coupling and Intermolecular Charge Transfer. *Chem. Rev.* **2018**, *118*, 7069–7163.

(41) Chenu, A.; Christensson, N.; Kauffmann, H. F.; Mančal, T. Enhancement of Vibronic and Ground-State Vibrational Coherences in 2D Spectra of Photosynthetic Complexes. *Sci. Rep.* **2013**, *3*, 2029.

(42) Dijkstra, A. G.; Prokhorenko, V. I. Simulation of Photo-Excited Adenine in Water with a Hierarchy of Equations of Motion Approach. *J. Chem. Phys.* **2017**, *147*, 064102.

(43) Green, D.; Camargo, F. V. A.; Heisler, I. A.; Dijkstra, A. G.; Jones, G. A. Spectral Filtering as a Tool for Two-Dimensional Spectroscopy : A Theoretical Model . **2018**, *122*, 6206–6213.

(44) Gelin, M. F.; Egorova, D.; Domcke, W. Efficient Method for the Calculation of Time- and Frequency-Resolved Four-Wave Mixing Signals and Its Application to Photon-Echo Spectroscopy. *J. Chem. Phys.* **2005**, *123*, 164112.

(45) Gelin, M. F.; Egorova, D.; Domcke, W. Efficient Calculation of Time- and Frequency-Resolved Four-Wave-Mixing Signals. *Acc. Chem. Res.* **2009**, *42*, 1290–1298.

(46) Leng, X.; Yue, S.; Weng, Y.-X.; Song, K.; Shi, Q. Effects of Finite Laser Pulse Width on Two-Dimensional Electronic Spectroscopy. *Chem. Phys. Lett.* **2017**, *667*, 79–86.

(47) Frisch, M. J.; Trucks, G. W.; Schlegel, H. B.; Scuseria, G. E.; Robb, M. A.; Cheeseman, J. R.; Scalmani, G.; Barone, V.; Mennucci, B.; Petersson, G. A.; et al. Gaussian 09, Revision C.1. Gaussian, Inc., Wallingford CT 2009.

(48) Clark, A. E.; Qin, C.; Li, A. D. Q. Beyond Exciton Theory: A Time-Dependent DFT and Franck-Condon Study of Perylene Diimide and Its Chromophoric Dimer. *J. Am. Chem. Soc.* **2007**, *129*, 7586–7595.

(49) Kjellberg, P.; Brüggemann, B.; Pullerits, T. Two-Dimensional Electronic Spectroscopy of an Excitonically Coupled Dimer. *Phys. Rev. B - Condens. Matter Mater. Phys.* **2006**, *74*, 1–9.

(50) Lide, D. R. *CRC Handbook of Chemistry and Physics*, 85th ed.; CRC Press: New York, 2004.

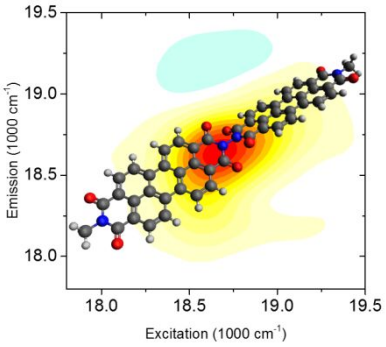
19.5
19.0
18.5
18.0
Emission (1000 cm-1)
18.0
18.5
19.0
19.5
Excitation (1000 cm-1)

TOC Graphic